Fabrication and biosensing with graphene edges

Gao, J.

Chapter 1

Introduction

Role of defects in sensing applications with graphene

1.1 Introduction

Graphene can have imperfections. Since its first isolation by Andre Geim and Konstantin Novoselov in 2004[1], graphene has attracted intense interest in nanoelectronics owing to its extraordinary carrier mobility and large functionalizable surface.[2-5] These properties make graphene an ideal transduction channel in field-effect transistor (FET) biosensors, which convert molecular binding events at the graphene–electrolyte interface directly into changes in graphene conductance with high sensitivity and rapid response[6,7]. Graphene field-effect transistors (Gr-FET) have been shown to detect a broad range of analytes by monitoring shifts in source–drain current or Dirac point[8,9], including nucleic acids[10,11], antibodies[12], whole cells[13,14], and even pH fluctuations[15,16]. Compared to conventional assays such as ELISA[17], PCR[18], and gel electrophoresis[19], Gr-FET biosensors operate label-free and enable real-time detection down to femtomolar levels[20]. In general, research on graphene biosensors has focused on graphene with uniform sp^2 configuration and nearly perfect lattice structures.[21] However, recent studies have revealed that various defects in graphene can be exploited to enhance the sensor performance of graphene,[22] such as edge defects, vacancies, grain boundaries, and wrinkles. Defects are structural or compositional deviations from the ideal two-dimensional, single-layer hexagonal honeycomb lattice of carbon atoms. Broken bonds from defects give rise to radical sites with readily available electrons, which exhibit unique electronic states and enhanced chemical reactivity.[23,24] These sites present unsaturated dangling bonds, local strain and distorted π-networks, which raise the local chemical potential and binding affinity and lower activation barriers for covalent and noncovalent interactions. For instance, edge defects can modulate carrier concentration through a doping effect; vacancy defects can adjust local energy levels via structural rearrangement, and grain boundaries or wrinkles can create localized electrostatic hotspots that facilitate charge transport and signal amplification.[25,26] Sensing at graphene defect refers to the strategy of exploiting intrinsic or engineered defects in the graphene lattice as active sites for molecular adsorption and transduction, such as vacancies, Stone–Wales transformations, edge sites, grain boundaries and wrinkles, thereby enabling or enhancing the sensor's response to target analytes. In this thesis, we review a structured framework by classifying graphene defects (point and line defects) based on their atomic structures, to then elucidate how these structural deviations may correlate with local electronic properties and chemical reactivity. This chapter therefore discusses literature-reported experimental and theoretical evidence across diverse sensing applications (ion, gas, DNA, protein) to show that defect engineering, particularly the utilization of edge sites, is a powerful strategy to enhance the sensitivity, selectivity of Gr-FET biosensors.[27-29]

1.1 Detection principle of graphene-field-effect biochemical sensors

A typical Gr-FET biosensor consists of three electrodes: the source (S), the drain (D), and the gate (G) (**Figure 1a**). A graphene monolayer bridges the source and drain electrodes, forming

a conductive channel. In a liquid-gated configuration, a reference electrode serves as the gate, applying a gate voltage to the electrolyte. The reference electrode is capacitively coupled to the graphene channel through an interfacial capacitance C, which comprises two series capacitances: the quantum capacitance of graphene (C_Q), and the electrical double-layer capacitance (C_{EDL}) of the electrolyte. C_Q originates from the finite density of electronic states (DOS) in graphene and reflects the ability of the graphene channel to accommodate additional charge carriers upon a change in electrochemical potential.[30] C_{EDL} arises from the redistribution of ions at the graphene–electrolyte interface upon application of a gate potential. It reflects the ability of the electrolyte to screen surface charges and is determined by the structure of the electrical double layer, which consists of a compact Stern layer and a diffuse layer described by Gouy–Chapman theory.[31] These two capacitive components determine the relationship between the surface potential change induced by biomolecular adsorption and the actual charge induced in the graphene channel. The effective gate voltage experienced by the channel is modulated by the potential drop across C_Q and C_{EDL}, such that charge generated by analyte binding directly translates into a change in carrier density Δn in the graphene sheet.

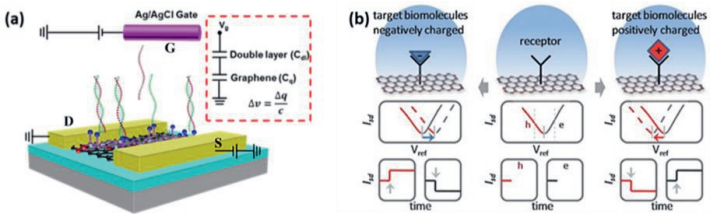

Figure 1. Schematic diagram of a graphene field-effect-transistor biosensor. **(a)** Structure diagram of graphene field effect transistor, which consists of a semiconductor layer and three electrodes: source, drain, and gate. The gate electrode is separated from the graphene layer by a gate dielectric (liquid). **(b)** The principle diagram of biosensor for immobilizing probe molecules and detecting charged molecules. Receptor molecules are anchored on the graphene surface in the upper schematic. The middle and lower panels show representative I_{ds}–V_{ref} and I_{ds}–t traces, respectively. The red "h" denotes measurements in the hole-transport regime, while the gray "e" indicates the electron-transport regime. The left and right sides of panel (b) illustrate the field-effect response caused by the binding of positively and negatively charged target biomolecules to the receptor, respectively. Such binding events, marked by gray arrows in the I_{ds} (t) traces, generate current variations and shift the I_{ds}–V_{ref} curves, as indicated by the blue arrows.[8]

The sensing mechanism is illustrated in **Figure 1b**: specific probe molecules are first immobilized on the graphene surface to capture charged target analytes, and their binding alters the local carrier density in the channel. This change shifts the drain–source current I_{ds} versus gate voltage V_{gs} characteristic, with positively charged analytes inducing hole depletion (n-type doping) that moves the Dirac point toward more negative V_{gs} and reduces I_{ds} in the hole-conduction regime, while negatively charged analytes cause the opposite shift and increase I_{ds}. The resulting current modulation can be approximated by:

$$\Delta I_{ds} = \frac{w}{l} V_{ds} e \mu \Delta n \propto N \quad (1)$$

where w and l are the channel width and length, V_{ds} is the source–drain bias, e is the elementary charge, μ is carrier mobility, and Δn which is proportional to the total number N of charged biomolecules adsorbing on the graphene surface. For instance, in miRNA detection, a complementary DNA probe is grafted onto the graphene surface; upon hybridization with target miRNA, the surface charge density changes, modulating the local electric field and channel conductance. Monitoring the resulting shifts in I_{ds} enables real-time, label-free quantification of miRNA concentration with high sensitivity.

1.2 Graphene defects

The sensitivity of Gr-FETs is influenced not only by the electric field effect induced by target molecules, but also by the intrinsic properties of graphene, particularly the defect states associated with its carbon lattice. This section will classify these defect types to reveal their specific roles in biosensing. As a two-dimensional material with a single-atom thickness, defects in graphene can be categorized into two main types: point defects and line defects. Point defects include Stone-Wales defects, vacancy defects, which disrupt the local atomic arrangement and modify the electronic and chemical properties of graphene.[32] Line defects consist of grain boundaries, wrinkles, and edge defects, which typically arise from the misalignment of graphene domains during growth or mechanical deformation and engineering.[33] Line defects also perturb the continuous sp^2-hybridized network of graphene, induce local lattice strain, and alter its electronic band structure and chemical reactivity.

From a sensing perspective, different types of graphene defects play distinct and mechanistically identifiable roles in signal generation. For point defects, including Stone–Wales and vacancy defects, they function primarily as localized adsorption spots and electronic perturbation centers.[34,35] Relative to pristine graphene, these defects introduce lattice distortion or undercoordinated carbon atoms that modify the local electronic structure and increase the adsorption strength of gas molecules, thereby improving gas-sensing performance.[36] In Stone–Wales defects, the 5–7 ring reconstruction generates a locally distorted site with altered electronic structure. DFT calculations showed that this defect has little effect on NH_3 adsorption, but strengthens NO_2 adsorption and causes significant deformation around the defect site, indicating that the sensing response depends on the match between the defect-induced electronic perturbation and the adsorbate's electron-accepting character.[37] In vacancy-defected graphene, the missing atoms create chemically altered sites with strong local reactivity; DFT on single-vacancy graphene shows that vacancies improved gas adsorption performance.[38] For line defects, edge defects primarily function as chemically active sites that enhance ion adsorption and interfacial charge transfer.[39] The unsaturated carbon atoms at graphene edges introduce dangling bonds and localized states that facilitate proton binding, making them particularly effective in pH sensing.[40] Experimental studies on edge-rich graphene devices, such as graphene mesh FETs, reported a 6-fold enhanced pH sensitivity compared to pristine basal-

plane graphene, with larger Dirac point shifts directly correlated to increased edge density.[41] This confirms that proton adsorption and charge modulation occur preferentially at edge defect sites rather than on the inert basal plane. In contrast, defects in the form of ripples,[42] wrinkles[43] or crumples[44] primarily act as electrostatic and geometric amplifiers of the sensing signal (the difference between ripples, wrinkles and crumples is described below in 1.2.2). Their out-of-plane deformation generates curvature-induced electric field concentration and modifies the local electrostatic environment, effectively increasing the coupling between charged analytes and the graphene channel. In crumpled graphene FETs, this effect has been experimentally shown to enable ultrasensitive nucleic acid detection down to the zeptomole range.[10]

1.2.1 Point defects

(1) Stone–Wales defect

The Stone-Wales (SW) defect, also known as the pentagon-heptagon (5|7) defect, is one of the most typical topological defects in graphene.[23] It arises when a C-C bond undergoes a 90° rotation around its midpoint, leading to the formation of adjacent pentagonal and heptagonal rings within the graphene lattice. As shown in **Figure 2a**, the authors observed this topological rearrangement in transmission electron microscopy, and DFT-optimized models reproduce the precise pentagon-heptagon topology reported experimentally (**Figure 2b**). In the case of SW defect, previous studies reported that imperfection can build a region with enhanced chemical reactivity such as nucleophilic properties.[37] This creates a desired site for binding of molecules.[32,45,46] DFT calculations further predict that SW defects can strengthen atomic and molecular adsorption due to enhanced charge transfer between the adsorbates and the defective graphene sheet,[37] which are particularly suitable for biochemical sensing applications.

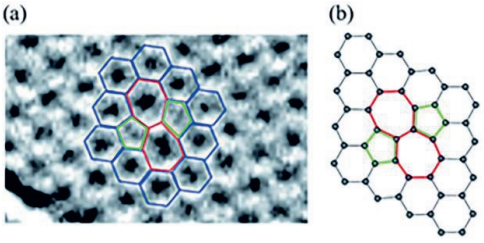

Figure 2. Stone–Wales defects: **(a)** Experimental TEM image showing a local topological defect produced by rotation of a C–C bond; the resulting 5–7–7–5 ring configuration and the associated displacement field are visible as distortions in the surrounding hexagonal lattice; **(b)** DFT calculated image, which reproduce the experimental contrast and local geometry, and highlight the rotated bond and the pentagon–heptagon pairs. The good agreement between experiment and simulation in both geometry and contrast validates the assignment of the observed feature to a Stone–Wales defect and provides insight into the defect-induced local structural and electronic perturbations. [23]

(2) Vacancy defects

Vacancy defects form when one or more carbon atoms are removed from the graphene lattice, creating atomic-scale voids that disrupt the continuous sp^2 network and introduce unsaturated dangling bonds.[23,33] **Figure 3a** presents a high-resolution transmission electron microscopy (HRTEM) image of a single-vacancy (SV) defect, in which the absence of one carbon atom produces a characteristic contrast variation and lattice relaxation in the surrounding hexagonal rings. The distortion of the neighboring C–C bonds reflect the reconstruction of the defect core and serves as direct experimental evidence of vacancy formation at the atomic scale.

The corresponding DFT-relaxed atomic structure of a SV defect in a ball-and-stick representation reported in **Figure 3b** is shown here. Upon removal of one carbon atom, the three adjacent carbon atoms initially possess dangling σ bonds; these atoms undergo reconstruction to form a stable 5–9 ring configuration, thereby lowering the defect formation energy.[36] The spin-polarized DFT model reproduces both the local lattice distortion and the contrast features observed in the HRTEM image.

Double vacancies (DV) arise either by coalescence of two SVs or by simultaneous removal of two neighboring carbons, and upon relaxation they typically reconstruct into 5-8-5 ring motifs without residual dangling bonds, resulting in greater thermodynamic stability but multiple possible metastable geometries.[47] As vacancies aggregate into larger clusters (multiple vacancies, MV), the defect evolves into extended pores or irregular voids whose perimeters contain a high density of under coordinated atoms.[48] Each additional vacancy increases the local strain and the number of reactive sites. The undercoordinated carbon atoms around vacancy defects have unpaired electrons, leading to higher local chemical potential and binding affinity, thus lowering the activation barrier for adsorption of target analytes markedly enhancing chemical adsorption and charge–transfer interactions.[49]

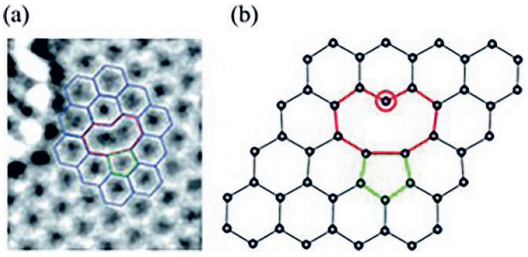

Figure 3. Single vacancy defect in graphene: **(a)** Experimental high-resolution TEM image showing the site of a single missing carbon atom in the graphene lattice; the vacancy causes local lattice relaxation and contrast changes in the adjacent hexagons. **(b)** DFT-relaxed atomic structure (shown as ball-and-stick). Depending on relaxation the vacancy may undergo Jahn–Teller reconstruction; the DFT model (spin-polarized where applicable) reproduces the observed lattice distortion and contrast. The comparison confirms the single-vacancy assignment and provides information on the local structural and electronic perturbation induced by the missing atom.[23,33]

1.2.2 Line defects

(1) Grain boundary defects

Grain boundary (GB) defects arise at the interfaces between adjacent graphene crystallites whose lattice orientations differ, yielding one-dimensional line defects.[50,51] The misorientation angle between neighboring grains governs the local defect topology, yet real GBs rarely form straight, periodic arrays; instead, they consist of irregular pentagon–heptagon (5|7) motifs arranged into polygonal chains with variable edge lengths and vertex angles.[23,33] At the atomic scale, the C–C bond lengths and bond angles within these boundaries deviate markedly from the ideal sp^2-hybridized lattice (bond length$\approx$0.142 nm), generating pronounced local strain and perturbing the electronic band structure.[52] The lattice misorientation and bond distortion at GBs break the continuous π-conjugated network of pristine graphene, generating localized electronic states within the band gap. These localized electronic states effectively regulate the charge carrier density and mobility of graphene, particularly modifying the electron density in the highest occupied molecular orbital (HOMO) and the lowest unoccupied molecular orbital (LUMO). When target analytes are adsorbed at GB active sites, efficient charge transfer occurs between the analytes and the graphene lattice, which significantly modulates the conductance of the graphene channel.

(2) Wrinkle defects

Graphene can exhibit a variety of out-of-plane morphological defects, which arise from mechanical deformation and depart markedly from the ideal two-dimensional lattice.[53,54] **Figure 4a** shows rippled graphene, characterized by low-amplitude, periodic or quasi-periodic height modulations with lateral wavelengths below ~10 nm. Such ripples are generally attributed to thermal fluctuations, intrinsic phonons, or weak interactions with the underlying substrate, and they introduce relatively small but spatially widespread curvature into the graphene sheet. In contrast, wrinkled graphene (**Figure 4b**) displays highly anisotropic ridge-like features formed by uniaxial or localized compressive strain. These wrinkles appear as sharp, linear bends that are typically 1–tens of nanometers wide, can reach heights of up to tens of nanometers, and often extend over hundreds of nanometers.[55] The pronounced curvature at wrinkle crests induces strong local strain gradients and breaks the in-plane symmetry of the lattice, giving rise to enhanced carrier localization and modified electrostatic environments along the wrinkle axis. **Figure 4c** illustrates crumpled graphene, which results from strong compression or mechanical manipulation and is characterized by highly disordered, multiscale folding and occasional overlap of graphene layers. Unlike ripples and wrinkles, crumples form dense, three-dimensional networks of interconnected folds, generating regions of extreme curvature and local stacking that strongly perturb both mechanical and electronic properties.

At the atomic scale, carbon atoms within these curved regions retain sp^2 hybridization, but

curvature imposes local tensile and compressive strain that distorts C–C bond lengths and angles.[56] Such curvature-induced strain concentrates electric fields at the apexes of wrinkles and crumples, enhancing charge redistribution and accelerating electron-transfer kinetics.[57] These combined mechanical and electronic perturbations have been shown to improve sensitivity in graphene-based FET biosensors and other nanoelectronic devices.[43]

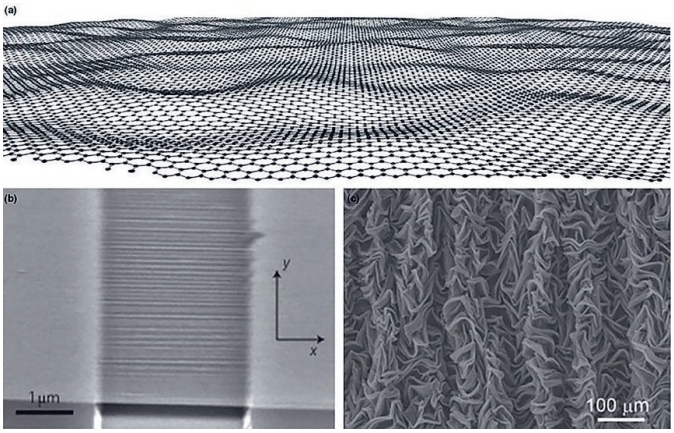

Figure 4. Rippled, wrinkled and crumpled graphene. **(a)** Rippled graphene: low-amplitude, periodic or quasi-periodic out-of-plane modulations likely arising from thermal fluctuations and/or weak substrate interactions. **(b)** Wrinkled graphene: anisotropic ridges produced by uniaxial or localized compressive strain, visible as sharp linear bends that span several nanometers. **(c)** Crumpled graphene: highly disordered, multi-scale folding that results from strong compression or mechanical manipulation and leads to large local curvature and overlap of graphene layers.[55]

(3) Edge defects

Graphene's edges interrupt the infinite sp^2 network of its hexagonal lattice, producing unsaturated σ- and π-dangling bonds that fundamentally alter both electronic structure and chemical reactivity. Two ideal edge terminations: zigzag and armchair exhibit sharply contrasting behaviors: zigzag edges support localized electronic states at the Fermi level, yielding metallic conduction and even edge magnetism,[58-60] whereas armchair edges lack mid-gap states and instead display a width-dependent semiconducting bandgap.[61] In both cases, undercoordinated carbon atoms form highly reactive sites, but zigzag terminations show greater radical character and binding affinity than armchair sites.[62] Real graphene edges rarely align perfectly along a single crystallographic direction and they instead form chiral edges, where zigzag and armchair segments alternate.[23,33,58] These complex edge geometries generate spatially varying densities of electronic states that dictate local adsorption energies and facilitate covalent or non-covalent functionalization, which are key mechanisms for enhancing sensitivity and selectivity in graphene-based biosensors.[32,48]

The contrasting electronic structures of zigzag and armchair edges arise from the distinct

boundary conditions each termination imposes on graphene's two-sublattice honeycomb lattice. In graphene, the electronic wavefunction carries a sublattice degree of freedom (commonly described as pseudospin) associated with the two inequivalent carbon sites (A and B sublattices) in the unit cell. At a zigzag edge, the termination occurs predominantly on a single sublattice, which breaks the A–B symmetry and prevents the low-energy wavefunction from cancelling at the boundary. This gives rise to quasi-localized π-electron states confined to the outermost carbon atoms, forming a nearly flat band at the Fermi level ($E = 0$) within an energy window of roughly $|k| < 2\pi/3a$ to π/a in reciprocal space, where a is the graphene lattice constant. The resulting sharp peak in the density of states (DOS) at the Dirac point translates directly into a large quantum capacitance (C_Q) at charge neutrality, producing the characteristic ∧-shaped C_Q profile. Armchair termination, by contrast, couples the two inequivalent Dirac valleys (K and K′) through boundary-induced intervalley scattering, which destroys the flat-band edge states and suppresses the DOS near the Dirac point. As a result, armchair edges exhibit a ∨-shaped C_Q profile closely resembling that of the graphene basal plane, with a near-zero capacitance minimum at the Dirac point.[58-60]

The difference in electronic structure also governs the chemical reactivity of the two edge types. Zigzag-terminated carbon atoms possess unsaturated dangling bonds with pronounced radical characters, arising from the singly occupied non-bonding states of the flat-band. This makes zigzag sites significantly more susceptible to covalent attack than armchair sites, whose wavefunction amplitudes at the boundary are strongly suppressed by intervalley mixing. In the context of diazonium salt functionalization—the covalent edge-modification strategy employed throughout this thesis—aryl radicals generated electrochemically react preferentially at zigzag carbons, where the higher local electron density lowers the activation barrier for C–C bond formation. Consequently, zigzag-rich edges support a higher surface density of covalently grafted linker groups per unit edge length, directly increasing the number of immobilized DNA probe molecules and thereby amplifying the biosensor response. The simultaneous advantage of zigzag edges in both quantum capacitance magnitude and covalent functionalization density makes them the ideal structural motif for the edge-based sensing platforms developed in the following chapters.[58-60]

1.3 Sensing at graphene defects

1.3.1 Ion sensing

Graphene based FET sensors are attractive for ion detection because the atomic thinness of graphene and high mobility enable strong transduction of interfacial charge perturbations into measurable electrical signals. Early work by Ang *et al.* reported that solution-gated epitaxial graphene on 6H–SiC exhibits pH-dependent Dirac-voltage shifts (pH 2–12), attributable to OH^-/H_3O^+ adsorption and thus enabling direct pH-to-voltage transduction.[63] Subsequent efforts

have extended this capability to real-time, high-resolution monitoring of multiple ionic species using large-area Gr-FET arrays and custom readout electronics; combining hundreds of sensing units with machine-learning calibration reported mitigate device-to-device variability and enable simultaneous quantification of K^+, Na^+ and Ca^{2+} in complex solutions.[64]

Despite these advances, several fundamental and practical challenges remain. Multiple studies indicated that an ideal, pristine graphene lattice exhibits negligible intrinsic response to protons, pristine basal planes do not provide effective adsorption sites for H^+; Consequently, the pH sensitivity reported in many graphene FET studies is predominantly mediated by structural or chemical defects rather than by the intact lattice itself.[65] [66] Mechanistically, defect sites can serve as adsorption sites for H_3O^+ and other ions, while the intact lattice on the graphene surface is unlikely to capture or adsorb these ions.[67,68] Photolithographic etching could introduce additional reactive edge sites. The role of edge defects in graphene mesh (GM) structures was studied in electrolyte-gated graphene mesh field-effect transistors (GM-FETs, **Figure 5a-b)**.[41] Compared to traditional Gr-FETs, GM-FETs show a larger Dirac point shift (30-100 mV/pH) and, in some cases, exceed the Nernst limit (59 mV/pH), as shown in **Figure 5c**. This enhanced response was ascribed to the strong adsorption of H^+ ions at edge defects, comprised of unsaturated carbon atoms. These edge sites act as highly active proton-binding centers, thereby amplifying the interfacial charge modulation and leading to an improved pH response.

Introducing additional H^+ binding sites via chemical functionalization is another effective strategy to improve the pH sensing sensitivity of Gr-FETs. Using diazonium electrochemistry, aminophenyl groups were covalently attached to graphene edges via diazonium salt electrochemical reactions, as shown in **Figure 5d**. This functionalization resulted in a stable substitution of phenyl groups at the edges, where the amino groups improved H^+ ion binding. The covalent attachment of these aminophenyl groups increased the pH sensitivity of the device compared to Gr-FETs and unmodified graphene edge sensors,[69] as shown in **Figure 5e**. A graphene-edge FET, and a graphene-edge FET functionalized by 4-aminophenyl diazonium was compared in **Table 1**. The Gr-FET with pristine surface device exhibits a sensitivity of 15.2 mV/pH. Introducing exposed graphene edges raises the sensitivity to 23.1 mV/pH, an improvement of 51.97% versus the Gr-FET with pristine surface device, consistent with enhanced H^+ adsorption at edge defects. Further functionalization with diazonium-derived aryl–NH_2 groups increases the sensitivity to 38.6 mV/pH, which is 153.94% higher than the Gr-FET with pristine surface. The large enhancement after functionalization is attributed to the high density of protonatable amine sites ($–NH_2$/$–NH_3^+$ equilibrium), which amplify the interfacial potential change produced by a given change in pH and thus increase the sensor's transduced signal.

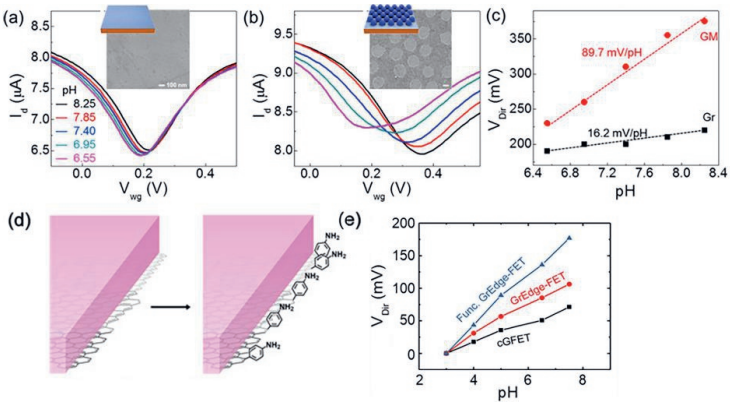

Figure 5. I_d-V_g curves for electrolyte-gated graphene-based FETs in aqueous solutions with pH ranging from 6.55 to 8.25, **(a)** pristine graphene device, **(b)** graphene mesh device. **(c)** Dependence of V_{Dirac} on pH for Gr-FET (black) and GM FET (red); solid lines indicate linear regression fits. In both devices, lowering the pH causes the Dirac point to move toward more negative potential. The Gr-FET shows a response of approximately 16.2 mV/pH. The GM-FET showed a much larger pH response, with a sensitivity of approximately 89.7 mV/pH. **(d)** Covalent electrochemical modification of the graphene edge. **(e)** Relative shift of the Dirac point as a function of pH in buffered solutions. The data measured with a Gr-FET are compared with a Gr edge-FET device in its initial state and after covalent modification.[41,69]

Table 1. pH sensitivity of three devices: graphene surface FET (Gr-FET), graphene-edge FET (Gr edge-FET), and Gr edge-FET after covalent functionalization with 4-aminophenyl diazonium (Func. Gr edge-FET). Edge exposure increases sensitivity by enhancing H^+ adsorption at reactive edge sites, and diazonium grafting (aryl–NH_2) further increases sensitivity by introducing protonatable amino groups.

Device	Sensitivity (mV/pH)
Gr-FET	15.2 ± 0.9
Gr edge-FET	23.1 ± 1.3
Func. Gr edge-FET	38.6 ± 1.5

1.3.2 Gas sensing

In 2007, Schedin *et al.* proposed that micrometer-sized graphene sensors can detect the adsorption and desorption of single gas molecules, producing step-like resistance changes due to single-electron carrier modulation.[70] Despite the demonstrated single-molecule detection capability of Gr-FETs, real applications remain hindered by inadequate selectivity. Therefore, enhancing the selectivity of gas sensors has become a major research focus. Functionalizing graphene to introduce specific chemical groups for targeted gas adsorption represents a highly promising strategy.

The edge regions of graphene nanoribbons (GNRs) can undergo chemical functionalization.

Aminopropyltriethoxysilane (APTES) molecules are covalently grafted onto the GNR edges to generate spatially isolated amino anchoring sites (**Figure 6a**). Upon hydrolysis, the ethoxysilane groups of APTES are converted to reactive silanols (Si–OH), which undergo condensation reactions with hydroxyl groups present at the graphene edges, forming stable Si–O–C covalent bonds and thereby introducing amino functionalities onto the GNR surface. To characterize the response selectivity of the sensors, the maximum gas response $\Delta R/R_b$ (%) of carbon nanotube (CNT), reduced graphene oxide (rGO), graphene nanoribbon, and APTES-functionalized GNR (GNR-APTES) sensors toward various analytes was measured, including NH_3, acetone, ethanol, propionaldehyde, CO_2, SO_2, and NO_2. In the reported comparison, the GNR sensor exhibited significantly higher responses than the CNT and rGO sensors toward acetone, ethanol, propionaldehyde, CO_2, SO_2 and NO_2 (**Figure 6b** and **6c**). Notably, after APTES functionalization, the GNR-APTES FET sensor demonstrated a particularly high response of 88% toward NO_2, which is about 6.3 times greater than its maximum response (~14%) to any of the other tested gases. At a low concentration of 0.125 ppm NO_2, the functionalized sensors showed a response of approximately 30% (**Figure 6d**), representing a 7-fold increase compared to unmodified GNR sensors. Compared with graphene basal plane-APTES FET sensors, which lack extensive edge exposure, GNR-APTES sensors achieved 93 times higher sensitivity.

The enhanced performance can be attributed to the combination of edge reactivity and amine functionalization. Density functional theory (DFT) calculations were performed to clarify the intrinsic mechanism underlying this performance enhancement, as the electronic structure of GNRs directly determines their electrical response to gas adsorption. DFT calculations indicate that APTES grafting increases the electron density in the highest occupied molecular orbitals (HOMO) of GNRs while leaving the overall band gap essentially unchanged (~1.0 eV). A higher HOMO electron density means the GNRs have more available electrons to transfer to NO_2 molecules, strengthening the charge transfer between GNRs and NO_2. This enhanced charge transfer directly amplifies the electrical signal generated by gas adsorption, thereby improving the sensor's sensitivity to NO_2. The introduced primary amine groups serve as additional adsorption sites with NO_2 binding energies comparable to those on the GNR basal plane, and gas molecule adsorption at these sites induces charge-density redistribution across the GNR plane.[71]

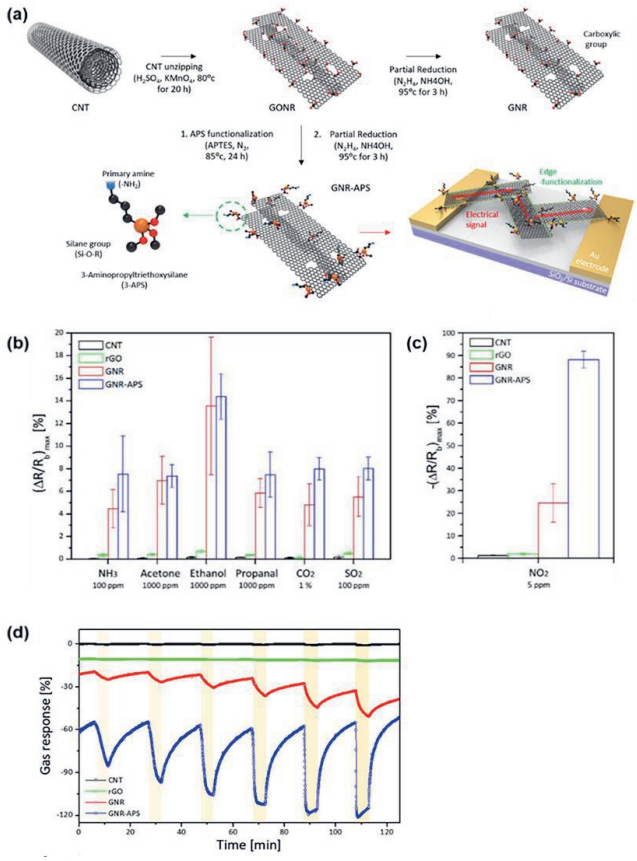

Figure 6. Preparation and sensing response of aminopropylsilane-functionalized graphene nanoribbons (GNR-APTES) **(a)** Schematic of the synthesis of GNR functionalized with APTES. GNR and GNR functionalized with aminopropylsilane (GNR-APS) were prepared using a scalable top-down process. First, GNR were synthesized via the chemically oxidative unzipping of multiwall carbon nanotube (MWCNT) bundles. Due to the intercalation of sulfuric acid on layers of MWCNTs, one-dimensional (1D) nanotubes were unzipped longitudinally, and the resultant graphene oxide nanoribbons (GONRs) were obtained with abundant oxygen functional groups, including hydroxyl (−OH), ketone (−C=O), and carboxylic (−COOH) groups. The GONR solution was chemically reduced using hydrazine as a reducing agent. To prepare GNR-APS, 3-aminopropyltriethoxysilane onto the GONRs at 85 °C under nitrogen (N_2) was grafted. Response selectivity of the CNT, rGO, GNR, and GNR-APS sensors for **(b)** NH_3, acetone, ethanol, propionaldehyde, CO_2, SO_2, and **(c)** NO_2. Here, R_b and ΔR represent the baseline resistance of each sensor and the change in resistance after exposure to gas molecules, respectively. **(d)** Real-time sensing performance of CNT, rGO, GNR, and GNR-APTES sensors for various concentrations of NO_2 from 0.125 to 5 ppm.[71]

1.3.3 DNA sensing

Gr-FETs have emerged as a powerful platform for label-free nucleic acid detection because they directly transduce the intrinsic negative charge of DNA molecules into electrical

signals.[72,73] Early demonstrations employed CVD-grown graphene in liquid-gated transistor configurations. After immobilization of single-stranded DNA (ssDNA) probes on the graphene surface, hybridization with complementary targets induced measurable shifts in the Dirac point, enabling detection limits down to ~10 pM.[74] To improve sensing performance in practical and complex biological environments, subsequent studies have focused on two major challenges: enhancing molecular-recognition specificity and sensitivity, and overcoming Debye screening in physiological ionic media. Debye screening is the electrostatic shielding effect caused by mobile ions in the electrolyte. When a charged biomolecule binds near the graphene surface, its electric field is partially neutralized by counterions in solution, so only the unscreened component can modulate the graphene channel conductance. The characteristic distance over which this screening occurs is the Debye length, which decreases with increasing ionic strength. In low-ionic-strength buffers, charges located farther from the surface can still be detected, whereas in physiological media such as PBS or serum, the shorter Debye length strongly attenuates the signal from biomolecular charges that are not very close to the graphene interface.[74]

One effective strategy to improve specificity is the incorporation of high-affinity recognition elements. For example, the CRISPR–Chip couples catalytically inactive dCas9–sgRNA complexes to a graphene channel, enabling direct, amplification-free electrical detection of target sequences with 1.7 femtomolar sensitivity and single-base mismatch resolution.[72] Similarly, a molecular-electromechanical system (MolEMS) uses a rigid DNA tetrahedron to locally passivate the surface and a flexible ssDNA cantilever as the sensing arm; electromechanical actuation brings target-bound molecules closer to the channel, enhancing transduction while suppressing nonspecific adsorption in biofluids.[75]

Despite these advances, the detection limit of Gr-FET DNA sensors remains fundamentally constrained by Debye screening, which attenuates the electric field generated by charged biomolecules in electrolyte solutions. Charges located beyond the Debye length do not effectively modulate the graphene channel, particularly under physiological ionic strengths. Defect engineering provides a powerful route to mitigate this limitation. By introducing controlled nanoscale crumples into monolayer graphene, Gr-FET DNA sensors can generate localized electrostatic “hot spots” that enhance sensitivity to nearby charges.[10] Compared with flat graphene, crumpled graphene exhibits convex regions where local curvature effectively extends the Debye screening length as shown in **Figure 7a**. As a result, a larger fraction of the DNA molecules resides within the effective Debye length, allowing their negative charges to more strongly influence the graphene channel conductance.

The fabrication process of crumpled Gr-FETs is shown in **Figure 7b**. Graphene was transferred onto a pre-strained polystyrene (PS) substrate, followed by thermal annealing at 110 °C to induce substrate shrinkage and generate uniform crumpling of the graphene layer. Scanning electron microscopy (SEM) images (**Figure 7c**) confirm the formation of hierarchical

nanoscale crumples over micrometer-scale channels.

In the reported study, these crumpled Gr-FETs exhibited extraordinary analytical performance, achieving detection limits down to the zeptomole (zM) range—for example, ~600 zM in buffer solutions and ~20 aM in human serum for millimeter-scale, uniformly crumpled devices. Computational modeling further supports the underlying mechanism: nanoscale deformations create spatially localized regions of enhanced electrostatic sensitivity, while curvature-induced modifications of the graphene band structure introduce an emergent bandgap.

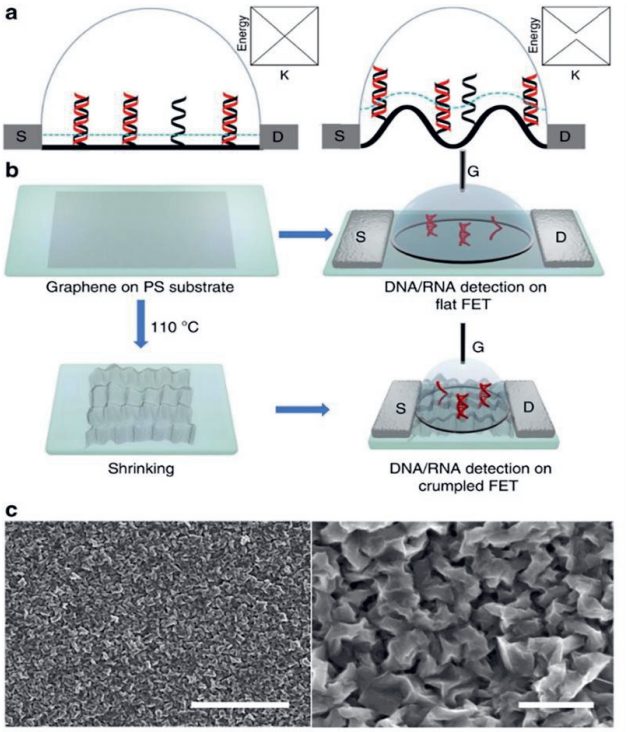

Figure 7. Fabrication of crumpled Gr-FETs. **(a)** Comparison of a planar graphene device and a crumpled graphene device in cross section. Probe DNA and complementary target DNA are shown on the graphene surface in black and red, respectively. The blue dashed curves indicate the Debye screening region in electrolyte. Owing to the local curvature of the crumpled graphene, a larger fraction of DNA molecules resides within the electrostatically active zone, leading to stronger transduction of the negative DNA charge. **(b)** fabrication of FETs and experimental process flow. Graphene on pre-strained PS substrate was annealed at 110 °C to shrink the substrate and crumple the graphene. **(c)** SEM images of crumpled graphene. The scale bar is 5 μm (left) and 500 nm (right).[10]

1.3.4 Protein sensing

Gr-FET biosensors have shown strong potential for protein detection in the literature. Typical Gr-FET protein biosensors employ surface linkers (*e.g.*, 1-pyrenebutyric acid succinimidyl

ester (PBASE), gold nanoparticles, aptamers) to immobilize capture probes or antigens on the graphene basal plane. Target protein binding then produces a Dirac point shift or source–drain current change. Representative demonstrations include ultrasensitive serological assays for SARS-CoV-2 antibodies (reported LOD ≈ 1 aM),[20] gold-nanoparticle-enhanced Gr-FET immunosensors (LOD≈2 fM),[76] and quantum-dot/ligand-exchanged Gr-FET functionalized with CD63 antibodies (LOD≈150 aM).[77]

However, in testing an actual biological sample, Gr-FET protein sensing has two practical limitations: nonspecific adsorption of background species on the graphene surface can interfere with analyte-specific signal; and Debye screening in ionic media weakens the electric field generated by large biomolecules when their charges are located outside the shielding length. Interface engineering has been used to address the first issue—for example, Nafion functionalized Gr-FET biosensor reduce nonspecific fouling and enable continuous cytokine monitoring in a broad dynamic range (reported range ~0.015-250 nM; LOD≈740 fM).[78] In this design, a porous, negatively charged Nafion layer isolates the graphene channel from the solution and effectively screens out nontarget species, such as lactic acid and amino acids. However, overcoming Debye screening is still challenging.

Defect-engineering of the graphene channel offers a strategy to tackle Debye screening limitations. Wrinkled or crumpled graphene with controlled defect content can form localized electrostatic "hot spots" and curvature-induced changes in the band structure that reduce effective charge screening and amplify current modulation. Using an interleukin-6 (IL-6) antibody on wrinkled, defect-containing Gr-FET in 1× PBS, aM-level IL-6 detection has been reported,[79] illustrating the potential of this approach.

Shortening the spatial distance between the biomarker and the graphene surface represents another effective route to alleviate Debye screening. Conventional Gr-FET biosensors typically rely on linker-mediated immobilization, in which molecules such as pyrenebutanoic acid succinimidyl ester (PSE) are used as chemical linkers to attach biorecognition elements onto the graphene surface. By contrast, linker-free immobilization of anti-tau antibodies onto patterned graphene edge defects (schematically illustrated in **Figure 8a–b**) yielded a ~3-fold enhancement in both charge-neutrality point shift and current modulation rate within the range of 10 fg/mL to 1 ng/mL, compared with conventional sensors using PSE linkers. These devices also exhibited ~4-fold higher current response rates in plasma samples from Alzheimer's patients relative to linker-based devices. This improved performance arises because patterning introduces a high density of edge defect sites that serve as direct anchoring points for the antibodies, obviating the need for intermediary linker chemistries such as PSE. In the linker-free architecture, antibodies are immobilized at edge defects, and the resulting interaction behaves analogously to defect-induced doping, enabling more efficient electron or hole transfer from antigen binding into the graphene channel. Furthermore, direct edge anchoring minimizes the spatial separation between the biorecognition event and the graphene

transducer surface, effectively reducing Debye screening effects in high ionic strength electrolytes (*e.g.*, physiological buffer or plasma) and thereby preserving signal transduction that would otherwise be attenuated in conventional linker-mediated immobilization.[80]

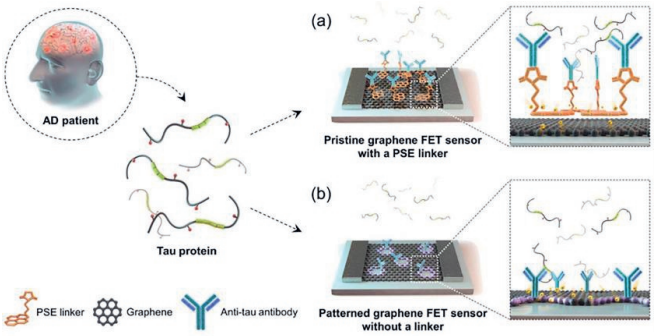

Figure 8. Illustration of antibody functionalization strategies for an electrolyte-gated graphene-based tau FET sensor. **(a)** For pristine graphene, antibodies were coupled through a pyrene-derived linker such as PBASE or a similar pyrene-terminated reagent, which enables receptor anchoring on the graphene surface. **(b)** For patterned graphene, no linker was required. The patterning process generates defect regions bearing oxygenated functional groups, providing direct chemical attachment sites for antibodies.[80]

1.3.5 Challenges

We have reviewed various defect-engineered Gr-FET sensing strategies, ranging from pH and gas detection to nucleic acid and protein assays, as shown in Table 2. Point defects are mainly applied in gas sensing, which regulate the local electronic state to enhance gas molecule adsorption and charge transfer. Line defects are widely used in the sensing of biomolecules such as pH, gas, DNA, protein and cells, which rely on their high-density active sites and local strain to improve the sensing response to biomolecules and ions. However, the inherently low density of naturally occurring defects limits the number of active adsorption sites and thus the ultimate sensitivity, while attempts to increase defect density invariably disrupt the sp^2 lattice, introduce carrier-scattering centers, degrade mobility and signal to noise ratio. Therefore, it is essential to develop non-destructive defect-amplification strategies and increase defect density without compromising the graphene's sensing performance.

Beyond the intrinsic trade-off between defect density and carrier mobility, several challenges remain for the practical deployment of defect-engineered graphene biosensors. Environmental factors such as pH, temperature, humidity, and ionic strength can significantly influence the electrical characteristics of graphene and introduce signal drift or measurement variability. In biological samples, nonspecific adsorption of proteins and other biomolecules may interfere with target recognition and reduce sensor selectivity. Furthermore, the stochastic nature of defect generation may lead to device-to-device variability, making large-scale manufacturing

and calibration challenging. Although defect engineering can substantially improve sensitivity by increasing the density of active sensing sites, maintaining long-term stability and reproducibility under real-world operating conditions remains an important challenge. Future research should therefore focus not only on enhancing sensitivity but also on improving environmental robustness, fabrication consistency, and long-term operational stability.

Table 2. Summary of the literature using defect-engineered graphene for sensing.

	Type	Sensing application
Point	Stone–Wales	CO[46,81], O_2[82], N_2[82]
	Vacancy	CO_2[38], NO_2[34], NH_3[34,35]
Line	Grain boundary	1,2-dichlorobenzene[83]
	Wrinkle	DNA[10], protein[84], cell[85]
	Edge	pH[86], NO_2[71], protein[80]

1.4 Aims and outline

In recent years, Gr-FET biosensors have attracted substantial interest, and several studies have reported that lattice imperfections can modulate adsorption, local density of states and device response. However, these reports are largely isolated observations and do not constitute a unified, device-oriented strategy for defect exploitation. Notably, defect-engineered graphene sensors still face several critical challenges. These include the trade-off between defect density and device electrical performance, difficulties in functionalizing defect sites, and high variability among sensors, which hinder their practical application. This thesis aims at taking advantage of the defects by forming graphene edge in sensing of Gr-FET biosensors. By harnessing and engineering intrinsic defects, we aim to enhance sensor sensitivity and stability.

In Chaper 2, to overcome the diffusion barrier of ultralow analyte concentrations to the sensor surface, we developed an edge-functionalized graphene nanoribbon field-effect transistor biosensor that integrates edge-localized dielectrophoretic (DEP) preconcentration. Graphene edges were functionalized by the electrochemical grafting of 4-N-Hydroxy succinimide benzene diazonium tetrafluoroborate salts (NHS-Ph-N_2^+) and were subsequently coupled to amine-terminated DNA probes. The atomically sharp graphene edges, together with the 12 nm HfO_2 dielectric layer between the graphene and the back-gate electrode, enables strong edge-localized DEP that concentrate target miRNA at the edge enabling detection of attomole concentrations of miRNA.

In Chapter 3, the fundamental trade-off between defect density and electronic performance in graphene-based biosensors is addressed. Although defect sites serve as highly active sites for molecular adsorption and signal transduction, their low density in pristine graphene limits the

number of accessible binding sites and thus constrains sensing sensitivity. Meanwhile, increasing defect density often compromises the intrinsic electrical properties of graphene by introducing carrier scattering centers. A polymer-mediated fracturing technique was therefore developed in which monolayer graphene is embedded in an epoxy matrix and then mechanically split at the midpoint. In this configuration, the graphene surface is fully encapsulated within a millimeter-thick polymer layer, preventing parasitic surface effects while enabling the precise formation of a clean graphene edge. This method isolates edge-specific quantum capacitance, as evidenced by an Λ-shaped capacitance profile that directly confirms the presence of localized defect states. Through potential-controlled diazonium grafting, graphene edges were functionalized with 4-N-Hydroxy succinimide (NHS) benzene diazonium tetrafluoroborate salts, enabling ultra-sensitive miRNA-21 detection at 1 fM with single-base discrimination, a 100-fold enhancement over conventional methods such as vinylsulfonated-polyamines (PA-VS), TIPS-Eth-ArN_2^+, and N-Heterocyclic Carbene (NHC) functionalization on graphene surface.

Chapter 4 describes a study to improve the density of graphene edge sites while maintaining high electrical performance. In addition, the device-to-device variability in graphene-based sensors by improving the reproducibility of the sensing interface. To achieve this, selectively functionalized graphene edges are used, where defects are naturally abundant, and while the basal plane is protected with a ceramic material. Graphene embedded in ceramic exhibits a quantum capacitance that is proportional to the density of states (DOS) and can therefore serve as the sensing transducer. This so-called edge-enhanced graphene quantum capacitor (eGQC) device allows us to reliably characterize the quantum capacitance (C_Q), which is proportional to the density of states specific to the graphene edges. The resulting eGQC biosensor with covalently functionalized graphene edges, demonstrates selective sensitivity towards miRNA and reusability for up to 100 cycles using oxygen plasma treatment without loss in performance. Remarkably, the standard deviation of calculated relative sensing response $\Delta C/C_0$ over the 100 times continuously miRNA detection concentrated at 41%.

In Chapter 5, a hybrid device architecture is developed by integrating a monolayer graphene channel with vertically aligned polyaniline (PANI) nanoarrays to combine the advantages of organic electrochemical transistors and high-mobility electronic conductors. In this design, a continuous monolayer graphene serves as a lateral charge transport channel, while the PANI nanoarrays act as the active sensing area. The PANI layer provides a volumetric ion–electron coupling medium, where ion penetration from the electrolyte modulates the local doping state of the polymer through protonation/deprotonation processes. DNA probes were immobilized on the PANI surface, enabling specific target recognition. Upon hybridization with target miRNA, the local electrostatic environment and protonation equilibrium within the PANI are perturbed, resulting in a change in its doping level and conductivity. This conductivity modulation in PANI is electrically coupled to the underlying graphene channel, which functions

as a high-mobility readout pathway that transduces small changes in carrier density into measurable variations in drain current. Based on this architecture, a graphene–PANI (Gr–PANI) organic electrochemical transistor biosensor was realized, achieving a detection limit down to 1 fM.

Chapter 6 summarizes the main findings of the thesis: various graphene edge-based biosensing platforms (including graphene nanoribbon, mechanically fractured monolayer graphene, ceramic-embedded reduced graphene oxide, and graphene-bridged polyaniline) were developed to detect miRNA with ultrahigh sensitivity, overcoming diffusion limits and being reusable under some conditions. Chapter 6 then outlines future outlooks, focusing on optimizing edge functionalization characterization, quantifying DNA density on the edge, and the use of the sensor in relevant biological conditions such as PBS and blood plasma.

1.5 References

1 Novoselov, K. S. *et al.* Electric Field Effect in Atomically Thin Carbon Films. *Science* **306**, 666-669 (2004). https://doi.org/10.1126/science.1102896

2 Geim, A. K. & Novoselov, K. S. The Rise of Graphene. *Nature Materials* **6**, 183-191 (2007). https://doi.org/10.1038/nmat1849

3 Geim, A. K. Graphene: Status and Prospects. *Science* **324**, 1530-1534 (2009). https://doi.org/10.1126/science.1158877

4 Novoselov, K. S. *et al.* A Roadmap for Graphene. *Nature* **490**, 192-200 (2012). https://doi.org/10.1038/nature11458

5 Barkan, T. *et al*. Mapping the Landscape for Graphene Commercialization. *Nature Reviews Physics* **6**, 646-647 (2024). https://doi.org/10.1038/s42254-024-00754-9

6 Pannone, A. *et al.* Robust Chemical Analysis with Graphene Chemosensors and Machine Learning. *Nature* **634**, 572-578 (2024). https://doi.org/10.1038/s41586-024-08003-w

7 Xue, M. *et al.* Integrated Biosensor Platform Based on Graphene Transistor Arrays for Real-time High-accuracy Ion Sensing. *Nature Communications* **13**, 5064 (2022). https://doi.org/10.1038/s41467-022-32749-4

8 Fu, W. *et al*. Sensing at the Surface of Graphene Field-Effect Transistors. *Advanced Materials* **29**, 1603610 (2017). https://doi.org/https://doi.org/10.1002/adma.201603610

9 Rohaizad, N. *et al*. Two-Dimensional Materials in Biomedical, Biosensing and Sensing Applications. *Chemical Society Reviews* **50**, 619-657 (2021). https://doi.org/10.1039/D0CS00150C

10 Hwang, M. T. *et al.* Ultrasensitive Detection of Nucleic Acids using Deformed Graphene Channel Field Effect Biosensors. *Nature Communications* **11**, 1543 (2020). https://doi.org/10.1038/s41467-020-15330-9

11 Zhang, Q. *et al.* Modular Fabrication of Microfluidic Graphene FET for Nucleic Acids Biosensing. *Advanced Science* **11**, 2401796 (2024). https://doi.org/https://doi.org/10.1002/advs.202401796

12 Ming, P. *et al.* A Drug Molecule-Modified Graphene Field-Effect Transistor Nanosensor for Rapid, Label-Free, and Ultrasensitive Detection of Estrogen Receptor α Protein. *Analytical Chemistry* **96**, 3454-3461 (2024). https://doi.org/10.1021/acs.analchem.3c04809

13 Krsihna, B. V., Ravi, S. & Prakash, M. D. Recent Developments in Graphene Based Field Effect Transistors. *Materials Today: Proceedings* **45**, 1524-1528 (2021). https://doi.org/https://doi.org/10.1016/j.matpr.2020.07.678

14 Zhang, X. *et al.* Dielectric-Modulated Biosensing with Ultrahigh-Frequency-Operated Graphene Field-Effect Transistors. *Advanced Materials* **34**, 2106666 (2022). https://doi.org/https://doi.org/10.1002/adma.202106666

15 Ren, H. *et al.* Field-Effect Transistor-Based Biosensor for pH Sensing and Mapping. *Advanced Sensor Research* **2**, 2200098 (2023). https://doi.org/https://doi.org/10.1002/adsr.202200098

16 Ohno, Y. *et al*. Electrolyte-Gated Graphene Field-Effect Transistors for Detecting pH and Protein Adsorption. *Nano Letters* **9**, 3318-3322 (2009). https://doi.org/10.1021/nl901596m

17 Klumpp, C. *et al.* Standardization of ELISA Protocols for Serosurveys of the SARS-CoV-2 Pandemic using Clinical and At-home Blood Sampling. *Nature Communications* **12**, 113 (2021). https://doi.org/10.1038/s41467-020-20383-x

18 Tombuloglu, H. *et al.* Multiplex Real-time RT-PCR Method for the Diagnosis of SARS-CoV-2 by Targeting Viral N, RdRP and Human RP Genes. *Scientific Reports* **12**, 2853 (2022). https://doi.org/10.1038/s41598-022-06977-z

19 Figueroa, S. *et al.* High Sensitivity-low Cost Detection of SARS-CoV-2 by Two Steps End Point RT-PCR with Agarose Gel Electrophoresis Visualization. *Scientific Reports* **11**, 21658 (2021). https://doi.org/10.1038/s41598-021-00900-8

20 Kang, H. *et al.* Ultrasensitive Detection of SARS-CoV-2 Antibody by Graphene Field-Effect Transistors. *Nano Letters* **21**, 7897-7904 (2021). https://doi.org/10.1021/acs.nanolett.1c00837

21 Bellunato, A. *et al*. Chemistry at the Edge of Graphene. *ChemPhysChem* **17**, 785-801 (2016). https://doi.org/https://doi.org/10.1002/cphc.201500926

22 Cho, H. *et al*. Chemical and Biological Sensors Based on Defect-Engineered Graphene Mesh Field-effect Transistors. *Nano Convergence* **3**, 14 (2016). https://doi.org/10.1186/s40580-016-0075-9

23 Bhatt, D. *et al*. Various Defects in Graphene: a Review. *RSC Advances* **12**, 21520-21547 (2022). https://doi.org/10.1039/D2RA01436J

24 Jiang, D. *et al*. Unique Chemical Reactivity of a Graphene Nanoribbon's Zigzag Edge. *The Journal of Chemical Physics* **126**, 134701 (2007). https://doi.org/10.1063/1.2715558

25 Girit, Ç. Ö. *et al.* Graphene at the Edge: Stability and Dynamics. *Science* **323**, 1705-1708 (2009). https://doi.org/10.1126/science.1166999

26 Zhang, X. *et al*. The Edges of Graphene. *Nanoscale* **5**, 2556-2569 (2013). https://doi.org/10.1039/C3NR34009K

27 Wang, X. *et al.* Targeting ADAR1 with a Small Molecule for the Treatment of Prostate Cancer. *Nature Cancer* **6**, 474–492 (2025). https://doi.org/10.1038/s43018-025-00907-4

28 Zhou, Y. *et al.* Tumor Biomarkers for Diagnosis, Prognosis and Targeted Therapy. *Signal Transduction and Targeted Therapy* **9**, 132 (2024). https://doi.org/10.1038/s41392-024-01823-2

29 Tenchov, R. *et al.* Biomarkers for Early Cancer Detection: A Landscape View of Recent Advancements, Spotlighting Pancreatic and Liver Cancers. *ACS Pharmacology & Translational Science* **7**, 586-613 (2024). https://doi.org/10.1021/acsptsci.3c00346

30 Xia, J. *et al*. Measurement of the Quantum Capacitance of Graphene. *Nature Nanotechnology* **4**, 505-509 (2009). https://doi.org/10.1038/nnano.2009.177

31 Huang, Y. *et al.* Ultrasensitive Quantum Capacitance Detector at the Edge of Graphene. *Materials Today* **73**, 38-46 (2024). https://doi.org/https://doi.org/10.1016/j.mattod.2023.12.011

32 Liu, L. *et al*. Defects in Graphene: Generation, Healing, and Their Effects on the Properties of Graphene: A Review. *Journal of Materials Science & Technology* **31**, 599-606 (2015). https://doi.org/https://doi.org/10.1016/j.jmst.2014.11.019

33 Banhart, F. *et al*. Structural Defects in Graphene. *ACS Nano* **5**, 26-41 (2011). https://doi.org/10.1021/nn102598m

34 Lee, G. *et al*. Defect-engineered Graphene Chemical Sensors with Ultrahigh Sensitivity. *Physical Chemistry Chemical Physics* **18**, 14198-14204 (2016). https://doi.org/10.1039/C5CP04422G

35 Dandeliya, S. & Anurag, S. Defected Graphene as Ammonia Sensor: Theoretical Insight. *IEEE*

Sensors Journal **19**, 2031-2038 (2019). https://doi.org/10.1109/JSEN.2018.2884971

36 Pašti, I. A. *et al.* Atomic Adsorption on Graphene with a Single Vacancy: Systematic DFT Study Through the Periodic Table of Elements. *Physical Chemistry Chemical Physics* **20**, 858-865 (2018). https://doi.org/10.1039/C7CP07542A

37 Jovanović, A. *et al*. Reactivity of Stone-Wales Defect in Graphene Lattice – DFT study. *FlatChem* **42**, 100573 (2023). https://doi.org/https://doi.org/10.1016/j.flatc.2023.100573

38 Vallejo, E. & López, P. A. Strong Chemical Adsorption of CO_2 and N_2 on a Five-vacancy Graphene Surface. *Solid State Communications* **356**, 114934 (2022). https://doi.org/https://doi.org/10.1016/j.ssc.2022.114934

39 Yuan, W. *et al.* The Edge- and Basal-plane-specific Electrochemistry of a Single-layer Graphene Sheet. *Scientific Reports* **3**, 2248 (2013). https://doi.org/10.1038/srep02248

40 Tan, X. *et al*. Edge Effects on the pH Response of Graphene Nanoribbon Field Effect Transistors. *The Journal of Physical Chemistry C* **117**, 27155-27160 (2013). https://doi.org/10.1021/jp409116r

41 Kwon, S. S. *et al.* Reversible and Irreversible Responses of Defect-Engineered Graphene-Based Electrolyte-Gated pH Sensors. *ACS Applied Materials & Interfaces* **8**, 834-839 (2016). https://doi.org/10.1021/acsami.5b10183

42 Fasolino, A. *et al*. Intrinsic Ripples in Graphene. *Nature Materials* **6**, 858-861 (2007). https://doi.org/10.1038/nmat2011

43 Wang, C. *et al*. Graphene Wrinkling: Formation, Evolution and Collapse. *Nanoscale* **5**, 4454-4461 (2013). https://doi.org/10.1039/C3NR00462G

44 El Rouby, W. M. A. Crumpled Graphene: Preparation and Applications. *RSC Advances* **5**, 66767-66796 (2015). https://doi.org/10.1039/C5RA10289H

45 Tiwari, S. K. *et al.* Stone–Wales Defect in Graphene. *Small* **19**, 2303340 (2023). https://doi.org/https://doi.org/10.1002/smll.202303340

46 Kumar, J., Ansh & Shrivastava, M. Stone–Wales Defect and Vacancy-Assisted Enhanced Atomic Orbital Interactions Between Graphene and Ambient Gases: A First-Principles Insight. *ACS Omega* **5**, 31281-31288 (2020). https://doi.org/10.1021/acsomega.0c04729

47 Alamdari, P. *et al*. Healing Double Vacancy Defects on Graphene: Reconstruction by C2 Adsorption. *Physical Chemistry Chemical Physics* **25**, 10759-10768 (2023). https://doi.org/10.1039/D2CP05233D

48 Tian, W. *et al*. A Review on Lattice Defects in Graphene: Types, Generation, Effects and Regulation. *Micromachines* **8,** 163-178 (2017). https://doi.org/10.3390/mi8050163

49 Ansari, R. *et al*. Fracture Analysis of MonolayerGraphene Sheets with Double Vacancy Defects via MD Simulation. *Solid State Communications* **151**, 1141-1146 (2011). https://doi.org/10.1016/j.ssc.2011.05.021

50 Cockayne, E. *et al.* Grain Boundary Loops in Graphene. *Physical Review B* **83**, 195425 (2011). https://doi.org/10.1103/PhysRevB.83.195425

51 Yazyev, O. V. & Louie, S. G. Topological Defects in Graphene: Dislocations and Grain Boundaries. *Physical Review B* **81**, 195420 (2010). https://doi.org/10.1103/PhysRevB.81.195420

52 Ahmad, W. *et al*. Introduction, Production, Characterization and Applications of Defects in Graphene. *Journal of Materials Science: Materials in Electronics* **32**, 19991-20030 (2021). https://doi.org/10.1007/s10854-021-06575-1

53 Zhang, T., Li, X. & Gao, H. Defects Controlled Wrinkling and Topological Design in Graphene. *Journal of the Mechanics and Physics of Solids* **67**, 2-13 (2014). https://doi.org/https://doi.org/10.1016/j.jmps.2014.02.005

54 Qin, H. *et al*. Mechanical Properties of Wrinkled Graphene Generated by Topological Defects. *Carbon* **108**, 204-214 (2016). https://doi.org/https://doi.org/10.1016/j.carbon.2016.07.014

55 Deng, S. & Berry, V. Wrinkled, Rippled and Crumpled Graphene: an Overview of Formation mechanism, electronic properties, and applications. *Materials Today* **19**, 197-212 (2016). https://doi.org/https://doi.org/10.1016/j.mattod.2015.10.002

56 Zhu, W. *et al.* Structure and Electronic Transport in Graphene Wrinkles. *Nano Letters* **12**, 3431-3436 (2012). https://doi.org/10.1021/nl300563h

57 Long, F. *et al.* Characteristic Work Function Variations of Graphene Line Defects. *ACS Applied Materials & Interfaces* **8**, 18360-18366 (2016). https://doi.org/10.1021/acsami.6b04853

58 Jia, X. *et al*. Graphene Edges: a Review of Their Fabrication and Characterization. *Nanoscale* **3**, 86-95 (2011). https://doi.org/10.1039/C0NR00600A

59 Fujii, S. & Enoki, T. Nanographene and Graphene Edges: Electronic Structure and Nanofabrication. *Accounts of Chemical Research* **46**, 2202-2210 (2013). https://doi.org/10.1021/ar300120y

60 Ruffieux, P. *et al.* On-surface Synthesis of Graphene Nanoribbons with Zigzag Edge Topology. *Nature* **531**, 489-492 (2016). https://doi.org/10.1038/nature17151

61 Celis, A. *et al.* Graphene Nanoribbons: Fabrication, Properties and Devices. *Journal of Physics D: Applied Physics* **49**, 143001 (2016). https://doi.org/10.1088/0022-3727/49/14/143001

62 Casiraghi, C. *et al.* Raman Spectroscopy of Graphene Edges. *Nano Letters* **9**, 1433-1441 (2009). https://doi.org/10.1021/nl8032697

63 Ang, P. K. *et al*. Solution-Gated Epitaxial Graphene as pH Sensor. *Journal of the American Chemical Society* **130**, 14392-14393 (2008). https://doi.org/10.1021/ja805090z

64 Fakih, I. *et al.* Selective Ion Sensing with High Resolution Large Area Graphene Field Effect Transistor Arrays. *Nature Communications* **11**, 3226 (2020). https://doi.org/10.1038/s41467

65 Fu, W. *et al.* Graphene Transistors Are Insensitive to pH Changes in Solution. *Nano Letters* **11**, 3597-3600 (2011). https://doi.org/10.1021/nl201332c

66 Angizi, S. *et al.* Defect Engineering of Graphene to Modulate pH Response of Graphene Devices. *Langmuir* **37**, 12163-12178 (2021). https://doi.org/10.1021/acs.langmuir.1c02088

67 Jung, H. *et al.* Super-Nernstian pH Sensor Based on Anomalous Charge Transfer Doping of Defect-Engineered Graphene. *Nano Letters* **21**, 34-42 (2021). https://doi.org/10.1021/acs.nanolett.0c02259

68 Fakih, I. *et al*. Sensitive Precise Measurement with Large-Area Graphene Field-Effect Transistors at the Quantum-Capacitance Limit. *Physical Review Applied* **8**, 044022 (2017). https://doi.org/10.1103/PhysRevApplied.8.044022

69 Neubert, T. J. *et al*. pH Sensitivity of Edge-Gated Graphene Field-Effect Devices with Covalent Edge Functionalization. *ACS Applied Electronic Materials* **4**, 4668-4676 (2022). https://doi.org/10.1021/acsaelm.2c00880

70 Schedin, F. *et al.* Detection of Individual Gas Molecules Adsorbed on Graphene. *Nature Materials* **6**, 652-655 (2007). https://doi.org/10.1038/nmat1967

71 Cho, K. M. *et al.* Edge-Functionalized Graphene Nanoribbon Chemical Sensor: Comparison with Carbon Nanotube and Graphene. *ACS Applied Materials & Interfaces* **10**, 42905-42914

(2018). https://doi.org/10.1021/acsami.8b16688

72 Hajian, R. *et al.* Detection of Unamplified Target Genes via CRISPR–Cas9 Immobilized on a Graphene Field-effect Transistor. *Nature Biomedical Engineering* **3**, 427-437 (2019). https://doi.org/10.1038/s41551-019-0371-x

73 Dontschuk, N. *et al.* A Graphene Field-effect Transistor as a Molecule-specific Probe of DNA Nucleobases. *Nature Communications* **6**, 6563 (2015). https://doi.org/10.1038/ncomms7563

74 Dong, X. *et al*. Electrical Detection of DNA Hybridization with Single-Base Specificity Using Transistors Based on CVD-Grown Graphene Sheets. *Advanced Materials* **22**, 1649-1653 (2010). https://doi.org/https://doi.org/10.1002/adma.200903645

75 Wang, X. *et al*. Molecular-electromechanical System for Unamplified Detection of Trace Analytes in Biofluids. *Nature Protocols* **18**, 2313-2348 (2023). https://doi.org/10.1038/s41596

76 Mao, S. *et al*. Highly Sensitive Protein Sensor Based on Thermally-reduced Graphene Oxide Field-effect Transistor. *Nano Research* **4**, 921-930 (2011). https://doi.org/10.1007/s12274-011-0148-3

77 Chen, J. *et al.* Exosome Biosensor Based on Quantum Dots-Modified Field Effect Transistor. *IEEE Sensors Journal* **25**, 34355-34362 (2025). https://doi.org/10.1109/JSEN.2025.3593869

78 Wang, Z. *et al.* A Flexible and Regenerative Aptameric Graphene–Nafion Biosensor for Cytokine Storm Biomarker Monitoring in Undiluted Biofluids toward Wearable Applications. *Advanced Functional Materials* **31**, 2005958 (2021). https://doi.org/https://doi.org/10.1002/adfm.202005958

79 Hwang, M. T. *et al.* Ultrasensitive Detection of Dopamine, IL-6 and SARS-CoV-2 Proteins on Crumpled Graphene FET Biosensor. *Advanced Materials Technologies* **6**, 2100712 (2021). https://doi.org/https://doi.org/10.1002/admt.202100712

80 Kwon, S. S. *et al*. The Role of Graphene Patterning in Field-effect Transistor Sensors to Detect the Tau Protein for Alzheimer's disease: Simplifying the Immobilization Process and Improving the Performance of Graphene-based Immunosensors. *Biosensors and Bioelectronics* **192**, 113519 (2021). https://doi.org/https://doi.org/10.1016/j.bios.2021.113519

81 Yang, S. *et al.* The Improved CO Adsorption/sensing Performance of Stone-Wales Defected Graphene Doped with Fe: A DFT Study. *Physica E: Low-dimensional Systems and Nanostructures* **128**, 114603 (2021). https://doi.org/https://doi.org/10.1016/j.physe.2020.114603

82 Auzar, Z. *et al*. Preferable Binding Site of Gas Molecules on Graphene Nanoribbon with Stone–Wales Defect. *Materials Research Express* **4**, 025014 (2017). https://doi.org/10.1088/2053-1591/aa598a

83 Yasaei, P. *et al.* Chemical Sensing with Switchable Transport Channels in Graphene Grain Boundaries. *Nature Communications* **5**, 4911 (2014). https://doi.org/10.1038/ncomms5911

84 Mukherjee, P. *et al*. Deformed Graphene FET Biosensor on Textured Glass Coupled with Dielectrophoretic Trapping for Ultrasensitive Detection of GFAP. *Nanotechnology* **35**, 295502 (2024). https://doi.org/10.1088/1361-6528/ad3d65

85 Lim, D. *et al.* Wrinkled PDMS-Based Graphene Field Effect Transistor Biosensor. *ACS Applied Electronic Materials* **7**, 236-245 (2025). https://doi.org/10.1021/acsaelm.4c01701

86 Knopfmacher, O. *et al.* Nernst Limit in Dual-Gated Si-Nanowire FET Sensors. *Nano Letters* **10**, 2268-2274 (2010). https://doi.org/10.1021/nl100892y